

AD-A086 218 CALIFORNIA RESEARCH AND TECHNOLOGY INC WOODLAND HILLS F/8 18/3  
EFFECTS OF DEBRIS ENTRAINMENT AND MULTI-PHASE FLOW ON PLUG LOAD--ETC(U)  
SEP 78 M ROSENBLATT, G E CARPENTER DNA001-77-C-0239  
UNCLASSIFIED CRT-3150F DNA-4686F NL

F/4 18/3

SEP 78 M ROSENBLATT, G E CARPENTER

DNA001-77-C-0239

**DNA-4686F**

**NL**

AC  
4095-719

END  
DATE  
FILMED  
8-80  
DTIC

**(10) LEVEL II**

AD-E 300809 P

DNA 4686F

ADA 086218

# EFFECTS OF DEBRIS ENTRAINMENT AND MULTI-PHASE FLOW ON PLUG LOADING IN AN MX TRENCH

California Research & Technology, Inc.

6269 Variel Avenue

Woodland Hills, California 91367

15 September 1978

Final Report for Period 1 May 1977-31 October 1977

CONTRACT No. DNA 001-77-C-0239

APPROVED FOR PUBLIC RELEASE;  
DISTRIBUTION UNLIMITED.

DDC FILE COPY

THIS WORK SPONSORED BY THE DEFENSE NUCLEAR AGENCY  
UNDER RDT&E RMSS CODE B344077462 J24AAXYX95502 H2590D.

Prepared for

Director

DEFENSE NUCLEAR AGENCY

Washington, D. C. 20305

DTIC  
ELECTE  
JUL 8 1980  
S B D

80 4 8 005

Destroy this report when it is no longer  
needed. Do not return to sender.

PLEASE NOTIFY THE DEFENSE NUCLEAR AGENCY,  
ATTN: STTI, WASHINGTON, D.C. 20305, IF  
YOUR ADDRESS IS INCORRECT, IF YOU WISH TO  
BE DELETED FROM THE DISTRIBUTION LIST, OR  
IF THE ADDRESSEE IS NO LONGER EMPLOYED BY  
YOUR ORGANIZATION.



UNCLASSIFIED

SECURITY CLASSIFICATION OF THIS PAGE (When Data Entered)

REPORT DOCUMENTATION PAGE		READ INSTRUCTIONS BEFORE COMPLETING FORM
1. REPORT NUMBER DNA 4686F	2. GOVT ACCESSION NO. AD-A086 218	3. RECIPIENT'S CATALOG NUMBER 7
4. TITLE (and Subtitle) EFFECTS OF DEBRIS ENTRAINMENT AND MULTI-PHASE FLOW ON PLUG LOADING IN AN MX TRENCH.	5. TYPE OF REPORT & PERIOD COVERED Final Report, for Period 1 May 1977 - 31 October 1977	
7. AUTHOR(s) Martin/Rosenblatt Gene E./Carpenter Robert P./Bilyeu	6. PERFORMING ORG. REPORT NUMBER 3150F	
9. PERFORMING ORGANIZATION NAME AND ADDRESS California Research & Technology, Inc. 6269 Variel Avenue Woodland Hills, California 91367	8. CONTRACT OR GRANT NUMBER(s) DNA 001-77-C-0239	
11. CONTROLLING OFFICE NAME AND ADDRESS Director Defense Nuclear Agency Washington, D.C. 20305	10. PROGRAM ELEMENT PROJECT TASK AREA & WORK UNIT NUMBERS Subtask/J24AAXYX955-02	
14. MONITORING AGENCY NAME & ADDRESS (if different from Controlling Office) 14. 12 3154F	12. REPORT DATE 15 September 1978	
	13. NUMBER OF PAGES 44	
	15. SECURITY CLASS (of this report) UNCLASSIFIED	
16. DISTRIBUTION STATEMENT (of this Report) Approved for public release; distribution unlimited.		
17. DISTRIBUTION STATEMENT (of the abstract entered in Block 20, if different from Report)		
18. SUPPLEMENTARY NOTES This work sponsored by the Defense Nuclear Agency under RDT&E RMSS Code B344077462 J24AAXYX95502 H2590D.		
19. KEY WORDS (Continue on reverse side if necessary and identify by block number) MX Debris Entrainment Multi-phase Flow Uncertainties Mixtures Trench Wall Ablation		
20. ABSTRACT (Continue on reverse side if necessary and identify by block number) The 1 1/2-D version of the multi-phase DICE code was used to analyze the flow of hot air and wall debris in covered MX trenches after an on-line burst. In DICE, debris particles are coupled to the air flow by thermal and drag mechanisms. The objective was to examine the effects of major uncertainties in the timing and magnitude of wall removal and debris entrainment upon the pressure and impulse loading on a rigid plug in the trench. The contributions to impulse due both to pressure loading and the momentum of the debris mass were considered.		

DD FORM 1 JAN 73 1473

EDITION OF 1 NOV 65 IS OBSOLETE

UNCLASSIFIED

SECURITY CLASSIFICATION OF THIS PAGE (When Data Entered)

UNCLASSIFIED

SECURITY CLASSIFICATION OF THIS PAGE(When Data Entered)

20. ABSTRACT (Continued)

Transfer of momentum and energy from the hot gas flow to the debris attenuates pressures and velocities. In all cases treated, the maximum pressure and impulse calculated on the plug were substantially lower than would be the case if no debris were present (i.e., if the flow in the trench consisted only of hot air). Where debris mass became entrained near the shock (say within 20-50 feet after the shock passes), plug loading was reduced by orders of magnitude. For example, entrainment of the debris from 0.15-in. of wall recession (with entrainment starting 18 feet behind the shock) reduced the maximum pressure on the plug from 6800 to 78 bars and the impulse from 24 to 3 bar-sec (as compared to air-only flow in the trench). Techniques to enhance early entrainment would be useful in reducing the design load on plugs. Debris not entrained until 100 feet or more behind the shock front has a much smaller effect on plug loading.

It is concluded that entrainment of debris from a modest thickness of wall recession into the flow in the trench can reduce the loading on a rigid plug in the tunnel by orders of magnitude, but this effect is quite sensitive to uncertainties in the entrainment processes.

UNCLASSIFIED

SECURITY CLASSIFICATION OF THIS PAGE(When Data Entered)

# TABLE OF CONTENTS

<u>Section</u>	<u>Page</u>
I. INTRODUCTION AND SUMMARY. . . . .	5
1.1 Background and Objectives. . . . .	5
1.2 Approach . . . . .	6
1.3 Summary and Conclusions. . . . .	8
II. ENTRAINMENT MODEL . . . . .	12
III. PLUG LOADING. . . . .	14
3.1 Effects of Entrainment Delay and Mass Loading. . . . .	14
3.2 Effects of Particle Size . . . . .	21
IV. IN-TRENCH RESPONSE. . . . .	24
4.1 Shock Pressure Attenuation . . . . .	24
4.2 Wall Recession . . . . .	25
APPENDIX A - PHYSICAL MODELS USED IN 1½-D DICE CALCULATIONS. . . . .	31
A.1 Aerodynamic Drag . . . . .	32
A.2 Thermal Interaction. . . . .	32
A.3 1½-D Venting and Wall Expansion. . . . .	33
REFERENCES . . . . .	38

ACCESSION for		
NTIS	White Section	<input checked="" type="checkbox"/>
DDC	Buff Section	<input type="checkbox"/>
UNANNOUNCED		<input type="checkbox"/>
JUSTIFICATION _____		
BY _____		
DISTRIBUTION/AVAILABILITY CODES		
Dist.	AVAIL.	and/or SPECIAL
A		-

## LIST OF ILLUSTRATIONS

<u>Figure</u>	<u>Page</u>
1. Processes Treated in $1\frac{1}{2}$ -D DICE Solutions. . . . .	7
2. Pressure-Time Histories on the Plug for Variations in the Mass Entrainment Parameter, $\beta(x)=\dot{T}/U_g$ . . . .	11
3. Mass Entrainment Parameter, $\beta$ , versus Distance Behind Shock Front, $x$ . . . . .	16
4. Maximum Pressure and Impulse Delivered to the Plug for Variations in Mass Entrainment Parameter, $\beta=\beta(x)$	17
5. Maximum Impulse ( $I_M$ ) and Shock Time of Arrival (TOA) versus Maximum Pressure ( $P_M$ ) at the Plug for Cases 1 through 6 . . . . .	18
6. A Comparison of Pressure and Impulse Time Histories using Two Wall Debris Entrainment Models. . . . .	20
7. Time Histories of Pressure Delivered to the Plug and Impulse for Variations in the Particle Size Distribution. . . . .	22
8. Shock Pressure vs Distance Attenuation Curves for the $L=18$ ft (Case 10) and $L=108$ ft (Case 2) Cases using a Step Entrainment Function with $\bar{\beta}=10^{-3}$ . . .	26
9. Shock Pressure vs Distance for Various Wall Debris Entrainment Parameters, $\bar{\beta}=.01$ , $.001$ , and $.0001$ . . .	27
10. Shock Pressure Attenuation with Distance for Variations in Entrained Particle Size Distribution.	28
11a. Wall Recession vs Distance Profiles for $\bar{\beta}=10^{-3}$ and $\bar{\beta}=10^{-4}$ . . . . .	29
11b. Wall Recession vs Distance Profiles with Entrained Particle Distributions of $D_p = .01$ cm and $D_p = .1$ , $1$ , and $10$ cm. . . . .	29
12. Extinction Times versus Particle Diameter for Radiative and Convective Heat Transfer Assuming a Small Dirt to Air Mass Ratio. . . . .	34

# LIST OF ILLUSTRATIONS (Cont'd)

<u>Figure</u>		<u>Page</u>
13a.	Equivalence of Circular and Square Trench Cross-sections . . . . .	35
13b.	Wall Expansion and Venting of Equivalent Square Trench . . . . .	35

## LIST OF TABLES

<u>Table</u>		<u>Page</u>
1.	Maximum Pressures and Impulses Delivered to Plug for Variations in Debris Entrainment Model . . . . .	15
2.	Maximum Pressures and Impulses Delivered to the Plug for Variations in Particle Size Distribution and Thermal Interaction. . . . .	23



## SECTION I

## INTRODUCTION AND SUMMARY

## 1.1 BACKGROUND AND OBJECTIVES

The survivability of any candidate M-X basing system must be evaluated using estimates of the hostile environment produced by nuclear bursts. Experimental and/or numerical simulations can be used to predict the physical characteristics of the hostile environment. These predictions and their associated uncertainties can then be used in analysis of the structural response of important elements in the basing system.

This report is concerned with one of the physical processes which affects the design environment in the buried-trench multiple aim point (MAP) basing concept<sup>1</sup>: After a nuclear burst within the trench or on the surface above a trench, a strong shock will be driven down the trench. The high velocity flow of shocked air in the trench will vaporize, melt, crush, and mix trench wall material (e.g., concrete, soil). Much of the debris\* will interact and become entrained into the flow, and this debris will attenuate the air flow velocity and shock strength by absorbing momentum and energy through drag and heat exchange. Our objective has been to examine the degree of this attenuation and the effects of debris entrainment (*and associated uncertainties*) on the pressure and impulse\*\* delivered to the plug in an MX trench.

---

\* We will use the term "debris" to include both vapor and condensed phase trench materials which become entrained into the high temperature air flow.

\*\* Impulse is delivered to the plug both by air pressure and by debris impact, i.e.,

$$I = \int_0^t P dt + \frac{\Sigma M_d U_d}{A}$$

## 1.2 APPROACH

The 1½-D version of the multi-phase DICE code\* was used to analyze the flow of hot air and debris in covered MX trenches, and to examine the effects of debris entrainment upon the loading imposed on a rigid plug in the trench 1800 feet from a 1 Mt on-line surface burst. For all the cases which were analyzed, it was assumed that the burst coupled 6.2 kt (all internal energy) to the air in the trench in the first 18 feet in both directions from the burst (i.e., 3.1 kt on each side). A 14 foot diameter trench buried 6 feet in the ground is the assumed configuration.

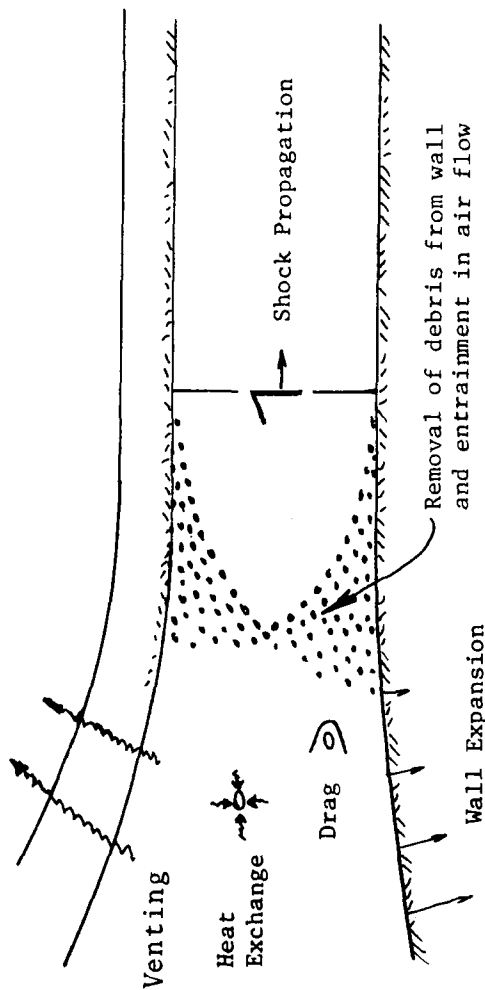
These 1½-D numerical simulations treated or took into consideration the phenomena which are shown in Figure 1, either through explicit calculations of the physical processes, or through prescription by separate models.

The processes by which material is removed from the trench wall and becomes entrained in the flow in the trench involve complex stress wave, thermodynamic, and turbulent boundary layer and mixing phenomena occurring under conditions which have not been accessible to experimental observation or investigation. Consequently there are major uncertainties, for any trench materials or construction, in the mass flux of debris off the walls, in the physical state of the debris (including size distribution of condensed-phase material), and in the timing of effective entrainment (mixing) of debris into the trench flow.

---

\* The basic DICE code<sup>2,3</sup> is a 2-D (axisymmetric) method to model the dynamics of formation of dust clouds following nuclear surface bursts. It is an implicit, compressible, Eulerian finite difference code which can treat the separate flow of different phases (condensed and vapor), material species, and particle sizes. The different groups and the basic medium (usually air) are mutually coupled by aerodynamic (drag) and thermodynamic (heat exchange) processes.

On-line Surface  
Burst



Processes treated explicitly

Shock generation and propagation in tunnel, and reflection from rigid plug

Hot air flow

Aerodynamic drag between debris and air flow

Heat exchange between debris and hot air

Melting and ablation of debris

Transfer of debris momentum to plug

Processes prescribed by separate models

Debris removal from trench walls by ablation, scouring, crushing, etc.

Debris particle sizes

Debris entrainment into air flow

Trench wall expansion  
Venting

Processes not treated

Turbulent mixing (except as crudely treated by varying nature of entrainment model)

Wall friction

Surface air blast

Individual debris particle impacts on plug

Figure 1. Processes Treated in 1½-D DICE Solutions.

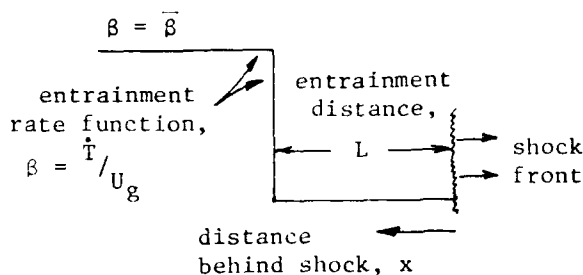
In the current program, we examined the *effects* of these uncertainties on pressure attenuation, trench wall recession, and the plug environment. This was done by numerical simulations in which several substantially different models were prescribed for the mass flux of debris, its size distribution, and the timing of its entry into the trench flow.

### 1.3 SUMMARY AND CONCLUSION

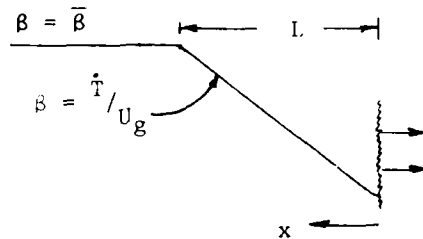
A baseline solution of the trench air flow with *no debris* (air-only) produced a maximum pressure of 6800 bars on the plug, and an impulse of 24 bar-sec. Eleven calculations were made of the trench flow with various debris entrainment models. In all cases, the maximum pressure, and the impulse on the plug (which includes the contributions of both pressure loading and debris mass) were substantially lower than in the air-only case. However, the magnitude of the reductions was strongly affected by the entrainment parameters.

Three aspects of debris entrainment were examined:

- o Entrainment delay (mixing length). Wall removal at a given station in the trench begins as soon as the shock passes. However, some interval of time (and therefore of distance behind the shock) elapses before debris is mixed with the flow over the entire cross-sectional area of the trench. To take this delay into consideration, we used the entrainment models in the following sketch to prescribe the behavior of the wall recession thickness,  $T$ , as a function of local gas flow velocity,  $U_g$ , and the distance behind the shock front,  $X$ .



Delayed-Step Entrainment



Ramp Entrainment

$$\dot{T} = \beta(x) U_g \text{ is the wall recession rate from debris entrainment}$$

The entrainment rate parameter,  $\bar{\beta}$ , is the maximum ratio of wall recession rate,  $\dot{T}$ , to the *local* velocity of the gas flow,  $U_g$ .

Plug loading was found to be very sensitive to the entrainment delay. Where significant entrainment occurred near the shock (say 20-50 feet behind the shock), plug loading was reduced by orders of magnitude. For example entrainment of the debris from 0.15-in. of wall recession (with entrainment starting 18 feet behind the shock) reduced the maximum pressure on the plug from 6800 bars to 78 bars and the impulse from 24 to 3 bar-sec (as compared to the air-only case).

- o Entrainment rate (and entrained mass). Increasing the entrainment rate (and mass) reduces loading on the plug; it may be possible to effectively quench the gas flow through techniques which enhance entrainment *within say 20-50 feet behind the shock*.

Figure 2 shows the effects of entrainment delay (mixing length) and the entrainment rate function,  $\beta = \dot{T}/U_g$ , on the pressure-time history at the plug for several cases. The important effects of an order of magnitude increase in the entrainment rate parameter can be seen by comparing Cases 3 and 5. Similarly, the effects of reducing the entrainment distance by a factor of two (from 108 to 54 feet) can be appreciated by comparing Case 5 to Case 6.

- o Debris size. Analysis in which the debris mass is initially divided evenly between 0.1, 1, and 10 cm particles were compared with cases using just .01 cm (= 100 $\mu$ ) particles. The smaller distribution reduced plug peak pressure loading by about a factor of 5 more than the larger distribution. Both drag and heat transfer depend on particle size; to determine which is more important, some analyses were repeated with *no* heat transfer being allowed between the gas and the particles. Plug loading was essentially the same, *with or without heat transfer*. This indicates that the addition of debris mass affects the mixed-phase flow dynamics primarily through drag interactions rather than through thermal interactions.

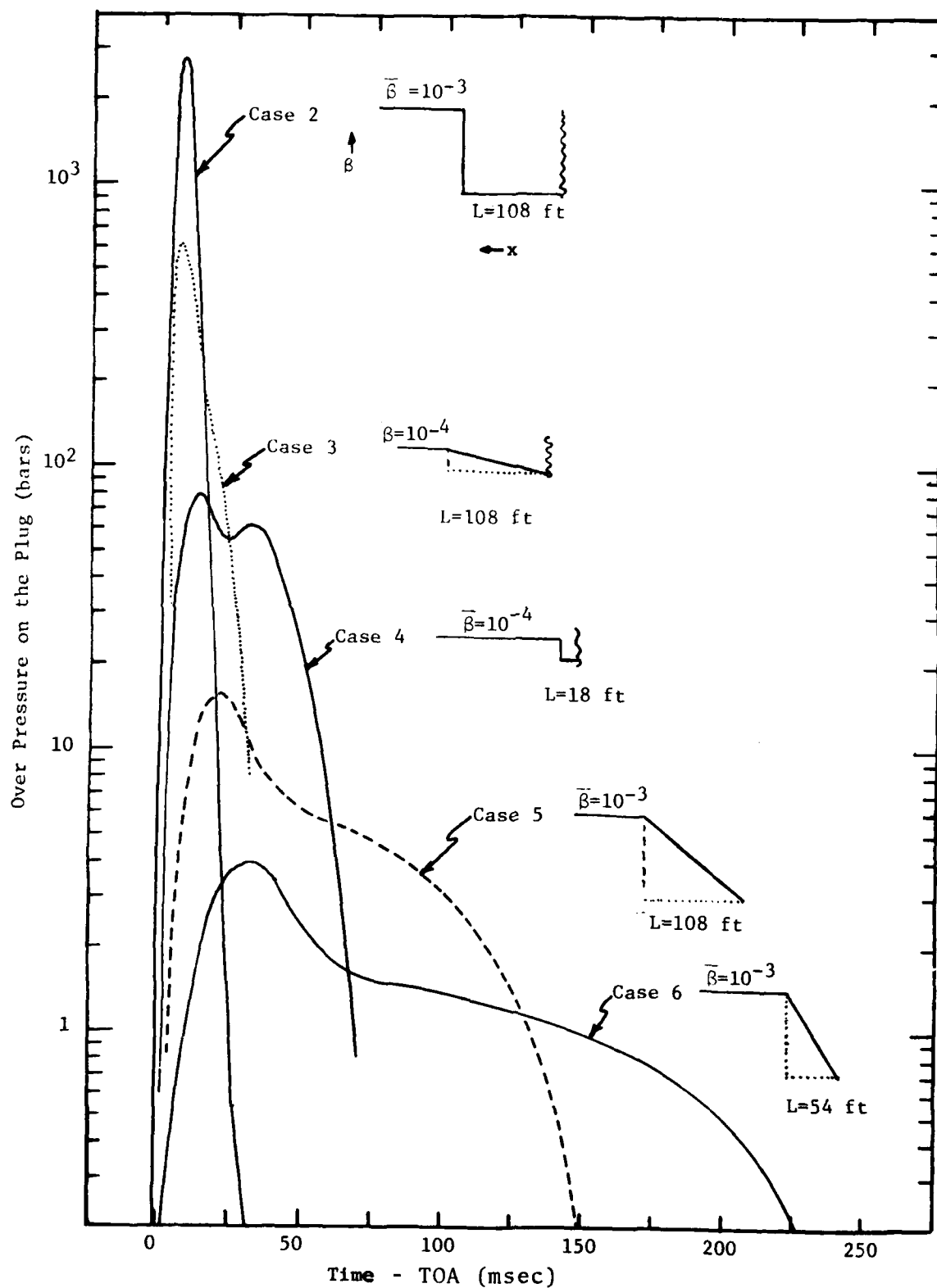
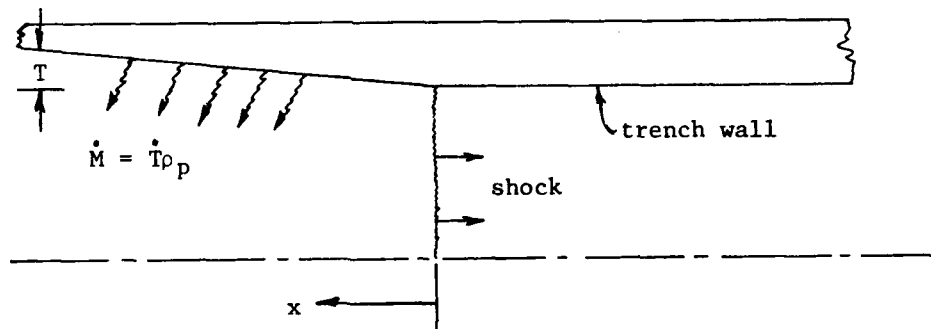


Figure 2. Pressure-Time Histories on the Plug for Variations in the Mass Entrainment Parameter,  $\beta(x) = T/U_g$ .

## SECTION II

### ENTRAINMENT MODEL

In the multi-phase DICE analyses, passage of the air shock is assumed to initiate removal of wall material and to start its mixing with the air flow. Debris is assumed to be solid-phase silica at the time of mixing, but thermal interactions can subsequently melt and vaporize the particles. The initial debris particle size is specified (sizes from  $100\mu$  to  $10\text{ cm}$  were considered). The entrainment delay and mass rate are specified by the following models:



$T$  = wall recession

$x$  = distance behind shock

$\rho_p = 2\text{ g/cm}^3$  = trench wall material density

$\dot{M}$  = mass entrainment rate per unit area at any trench station

$$= \dot{T} \rho_p = \beta \rho_p U_g$$

where  $\beta = \frac{\dot{T}}{U_g} \equiv$  entrainment rate parameter which is a function of  $x$

$U_g$  = local gas flow velocity



Note that both  $\beta$  and  $U_g$  are functions of the instantaneous distance of the trench station behind the shock front.

The variation of  $\beta$  with  $x$  was described by delayed step-function models and by ramp-function models. The parameters for several of the models used are shown in Figure 3, page 15.

The variation of  $U_g$  with  $x$  depends on the flow dynamics behind the shock. These flow dynamics are affected by the entrainment of debris; hence  $U_g$  is coupled to the entrainment delay and the entrainment mass rate,  $\dot{M}$ . This coupling is taken into consideration explicitly in the numerical calculations.

Models used in the DICE calculations for other processes, including aerodynamic drag, thermal interactions, and simulation of tunnel wall expansion and venting, are described in the Appendix.

### SECTION III

#### PLUG LOADING

##### 3.1 EFFECTS OF ENTRAINMENT DELAY AND MASS LOADING

Table 1 summarizes the time of arrival, maximum pressure, ( $P_M$ ) and impulse ( $I_M$ ) delivered to the plug for six variations in wall debris entrainment characteristics. Case 1, the limiting case with no debris (air only), was run for comparison\*. Cases 2 through 6 use the *entrainment rate parameters*  $\beta(x)$ , shown on Figure 3. Figure 4 lists the maximum pressures and impulses directly on the  $\beta(x)$  profiles, in order to illustrate the sensitivity of  $P_M$  and  $I_M$  to uncertainties in debris entrainment.

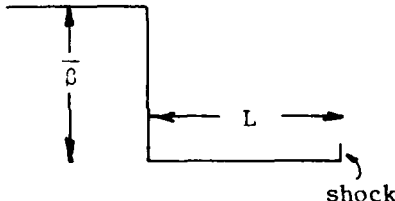

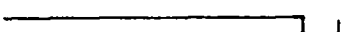

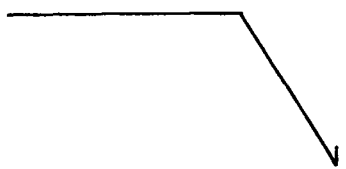
A comparison of the two delayed step-function cases (2 and 4) shows that introducing mass near the shock front is very effective in attenuating the plug  $P_M$  and  $I_M$ . When the "mixing length" ( $L$  in Table 1) was reduced from 108 feet to 18 feet, the peak pressure on the plug dropped from 2500 bars to 78 bars (factor of 32) and the impulse dropped from 12 bar-sec to 3 bar-sec (factor of 4). Similarly, results when ramp functions of  $\beta$  were used (Cases 3, 5, and 6) show a strong dependence on the debris entrainment characteristics near the shock front.

Figure 5 is a plot of impulse and time of arrival versus maximum pressure on the plug for Cases 1 through 6. The impulse delivered to the plug varies roughly with the .6 power of maximum pressure,  $I_M \sim (P_M)^{.6}$ , and the time of arrival varies roughly with the .3 power,  $TOA \sim (P_M)^{-.3}$ . The generality of these relationships is not known. However, if validated, these are significant

---

\* Results from the MARVEL test (2.1 kt burst in a 3.2-foot dia. tunnel) have shown that the air-only model is a poor representation of what actually happens. Some incorporation of wall ablation and scouring is needed to explain the MARVEL observations.

Table 1. Maximum Pressures and Impulses Delivered to Plug for Variations in Debris Entrainment Model.

Case	Entrainment Model $\beta = \beta(x) = \dot{T}/U_g$	Parameters		Plug Loading		
		$\bar{\beta}$	L (ft)	TOA (msec)	$P_M$ (bars)	$I_M$ (bar-sec)
1	Air Only (no debris)	-	-	26	6800	24
2		$10^{-3}$	108	29	2500	12
3		$10^{-4}$	108	42	621	6
4		$10^{-4}$	18	81	78	3
5		$10^{-3}$	108	140	16	0.8
6		$10^{-3}$	54	240	4	0.3

In all these debris models, total mass was initially divided equally between 0.1, 1, and 10 cm particles.

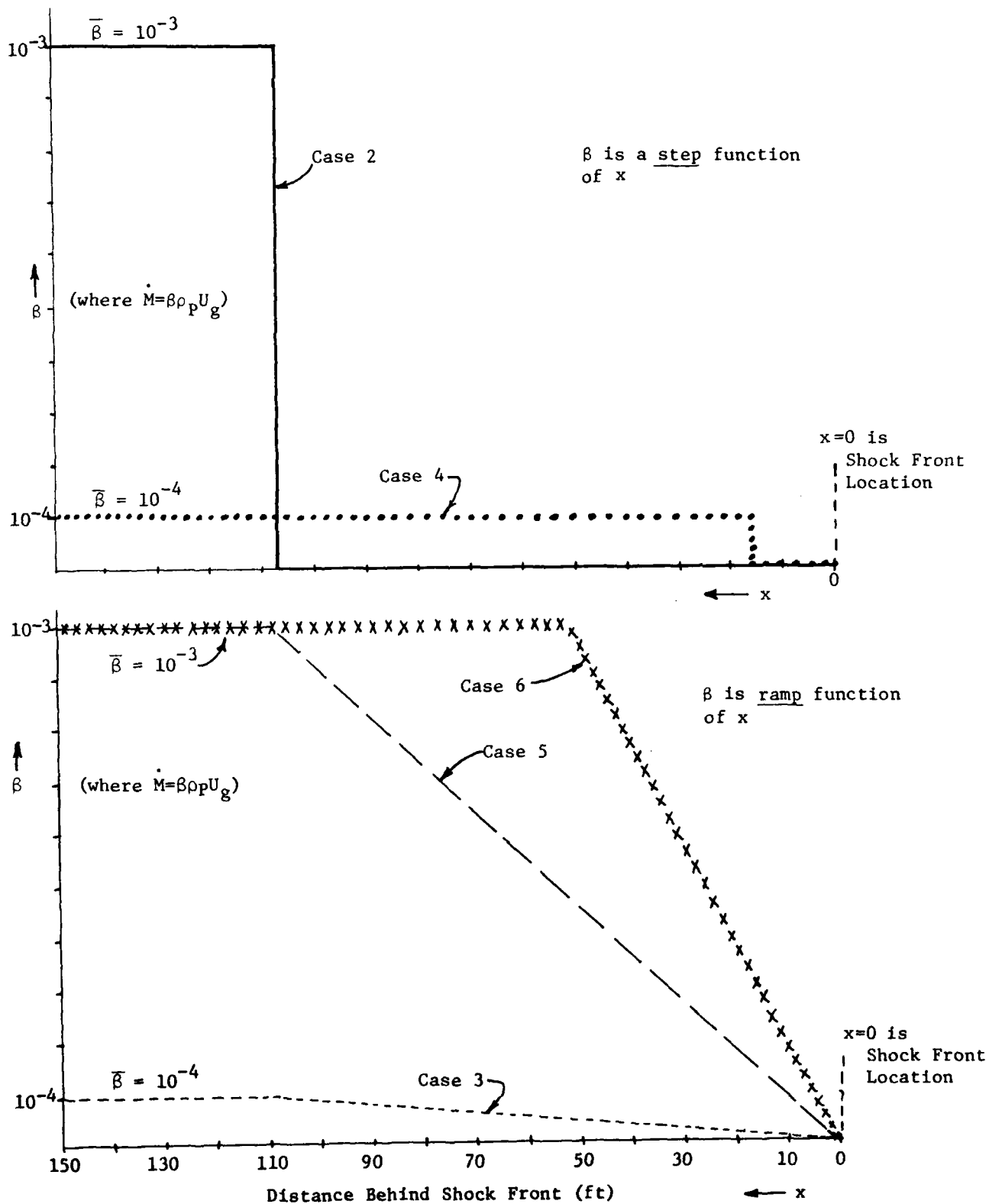


Figure 3. Mass Entrainment Parameter,  $\beta$ , versus Distance Behind Shock Front,  $x$ .

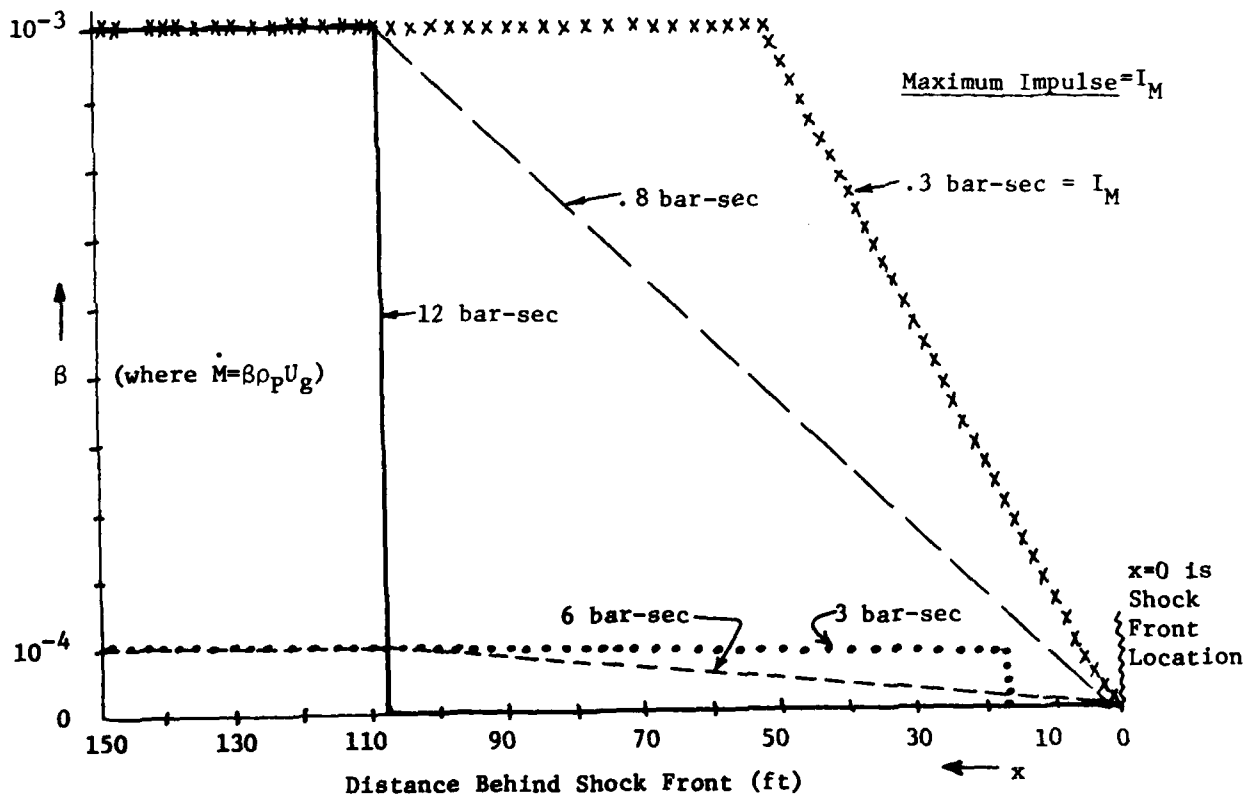
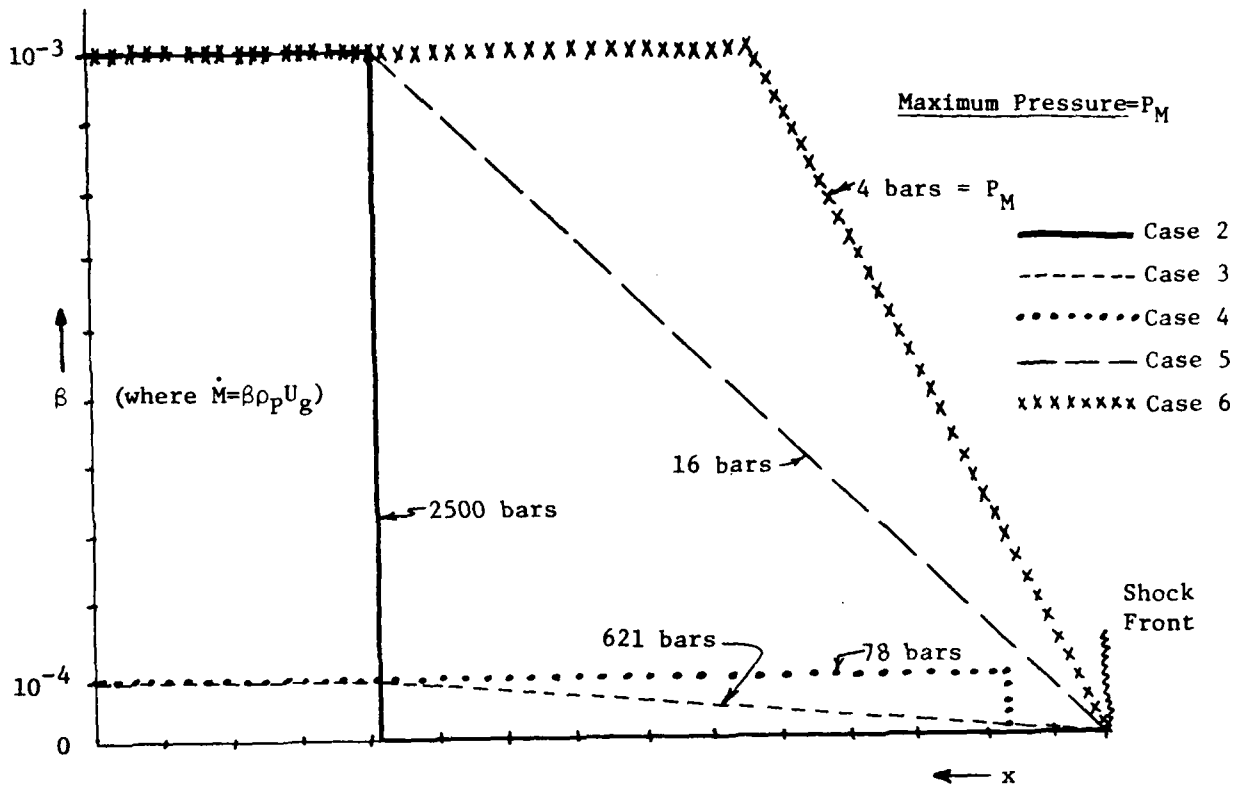


Figure 4. Maximum Pressure and Impulse Delivered to the Plug for Variations in Mass Entrainment Parameter,  $\beta = \beta(x)$ .

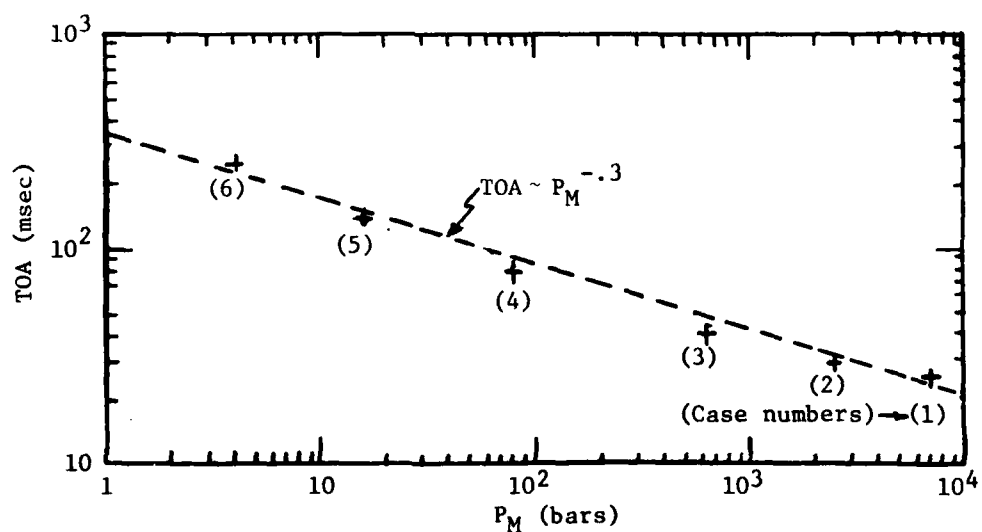
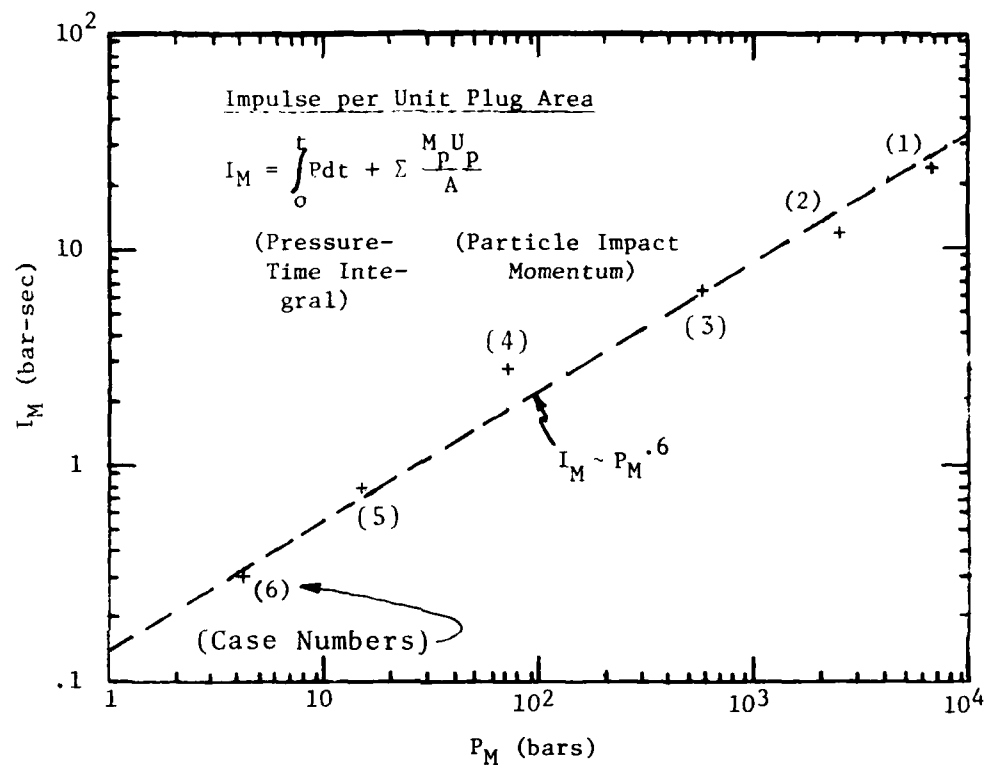


Figure 5. Maximum Impulse ( $I_M$ ) and Shock Time of Arrival (TOA) versus Maximum Pressure ( $P_M$ ) at the Plug for Cases 1 through 6 (see Table 1).

relationships in that they indicate debris uncertainties which lead to factors of 10 variations in  $P_M$  produce only factors of ~4 uncertainty in  $I_M$ .

The *time-resolved* pressures on the plug and the cumulative impulse delivered to the plug are shown in Figure 6 for two cases. Cases 2 and 5 differ in the treatment of the 108 feet behind the shock front. When a ramp dependence for  $\beta(x)$  (Case 5) is used in place of a delayed step function (Case 2) the following related effects are observed:

- o the maximum pressure is reduced by a factor of ~150.
- o the total impulse delivered to the plug is reduced by a factor of ~15.
- o the time of arrival increases by a factor of ~4 to 5.
- o the duration of the pressure pulse on the plug increases by a factor of ~4 to 5.

Figure 2 summarizes the sensitivity of the pressure loading to variations in the wall debris entrainment rate parameter  $\beta(x)$ . The pressure-time histories have been shifted to begin at the times of arrival in Table 1. The important effects (~ factor of 40 in  $P_M$ ) of an order of magnitude change in  $\beta = \dot{T}/U_g$  can be seen by comparing Case 3 ( $\bar{\beta} = 10^{-4}$ ) and Case 5 ( $\bar{\beta} = 10^{-3}$ ). Similarly, the effects (~ factor of 4) of reducing the mixing length  $L$  by a factor of 2 can be appreciated by comparing Case 5 ( $L=108$  feet) to Case 6 ( $L=54$  feet). *The plug loading characteristics ( $P$  vs time,  $P_M$ , and  $I_M$ ) are all sensitive to the entrainment of wall debris material near the shock front.*

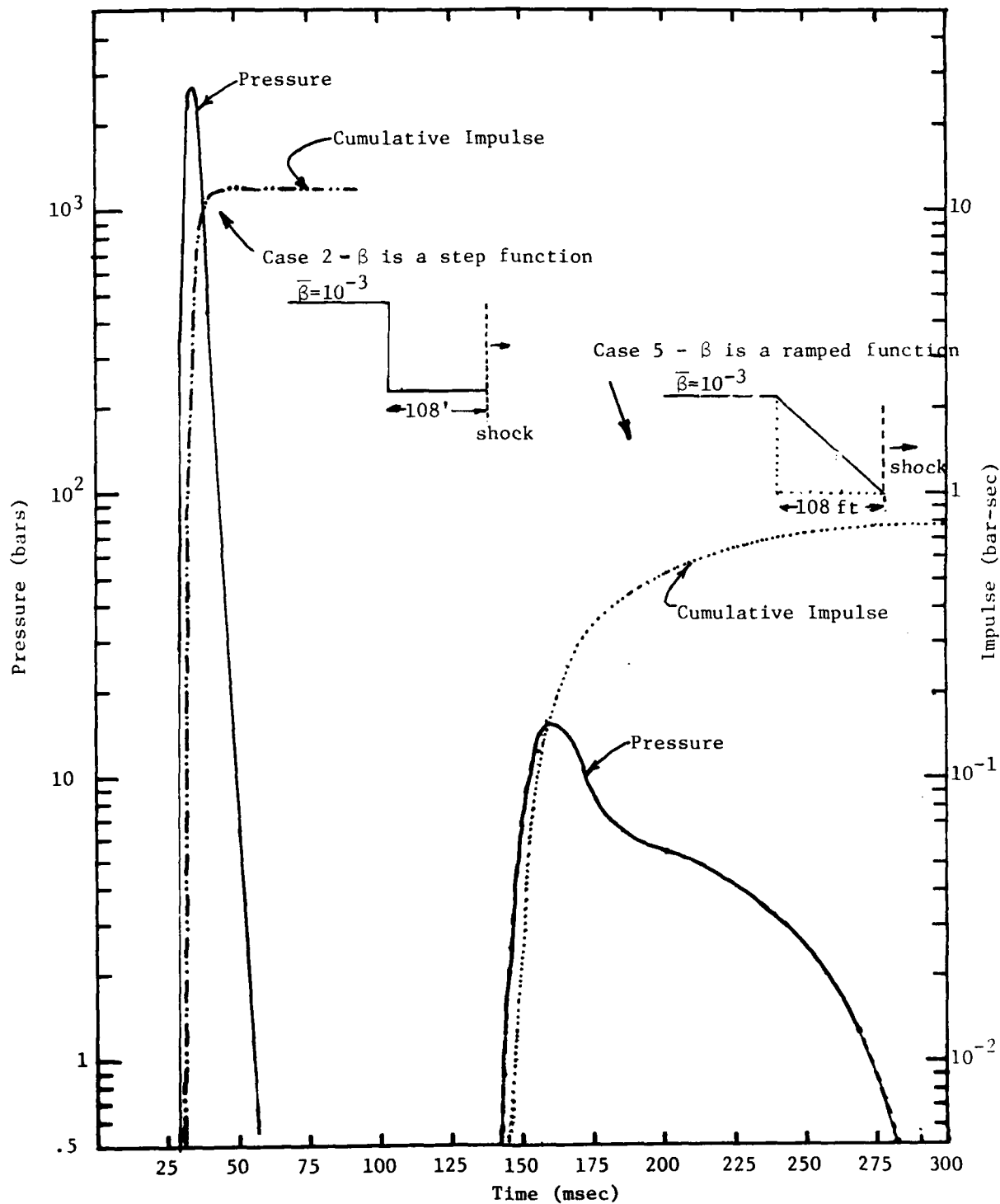


Figure 6. A Comparison of Pressure and Impulse Time Histories using Two Wall Debris Entrainment Models. (Plug is Located 1800 ft from a 1 Mton On-Line Surface Burst.)



### 3.2 EFFECTS OF PARTICLE SIZE

The multi-phase mixture of air, solid-liquid debris particles, and debris vapor interacts through drag and thermal mechanisms. The drag forces act on both the air and debris; these forces generally accelerate the debris material while decelerating the high velocity air. The thermal interactions involve exchanges of energy primarily through ablation. Both drag and thermal interactions are a strong function of solid/liquid *particle size*.

The influence of uncertainties in the particle size distribution is shown on Figure 7. The only difference between the two numerical simulations is that Case 7 uses a single debris particle size of  $D=100\mu = .01$  cm as compared to the nominal particle size distribution of  $D=.1, 1, \text{ and } 10$  cm particles\* used in Case 3.

Figure 7 shows that if wall debris is assumed to mix with the shocked air in "small" particles ( $D = 100\mu = .01$  cm), as compared to the nominal particle size distribution ( $D = .1, 1, \text{ and } 10$  cm), then the enhanced drag and thermal interactions will cause the maximum pressure to drop by an additional factor of  $\sim 5$ , and the impulse to drop by an additional factor of  $\sim 2$ .

In order to evaluate the relative importance of drag as compared to thermal interactions, two numerical simulations (Cases 8 and 9) were performed which ignored all thermal mechanisms, i.e. no ablation or conduction was allowed (similar to Cases 3 and 7 on Figure 7 except there are no thermal interactions). Table 2 summarizes the results of these numerical simulations.

---

\* In the nominal case, the mass is initially divided equally among each particle size group, i.e 1/3 of the mass is in .1 cm particles, 1/3 in 1 cm particles, and 1/3 in 10 cm particles. This nominal particle size distribution is used in all cases except Cases 7 and 9.

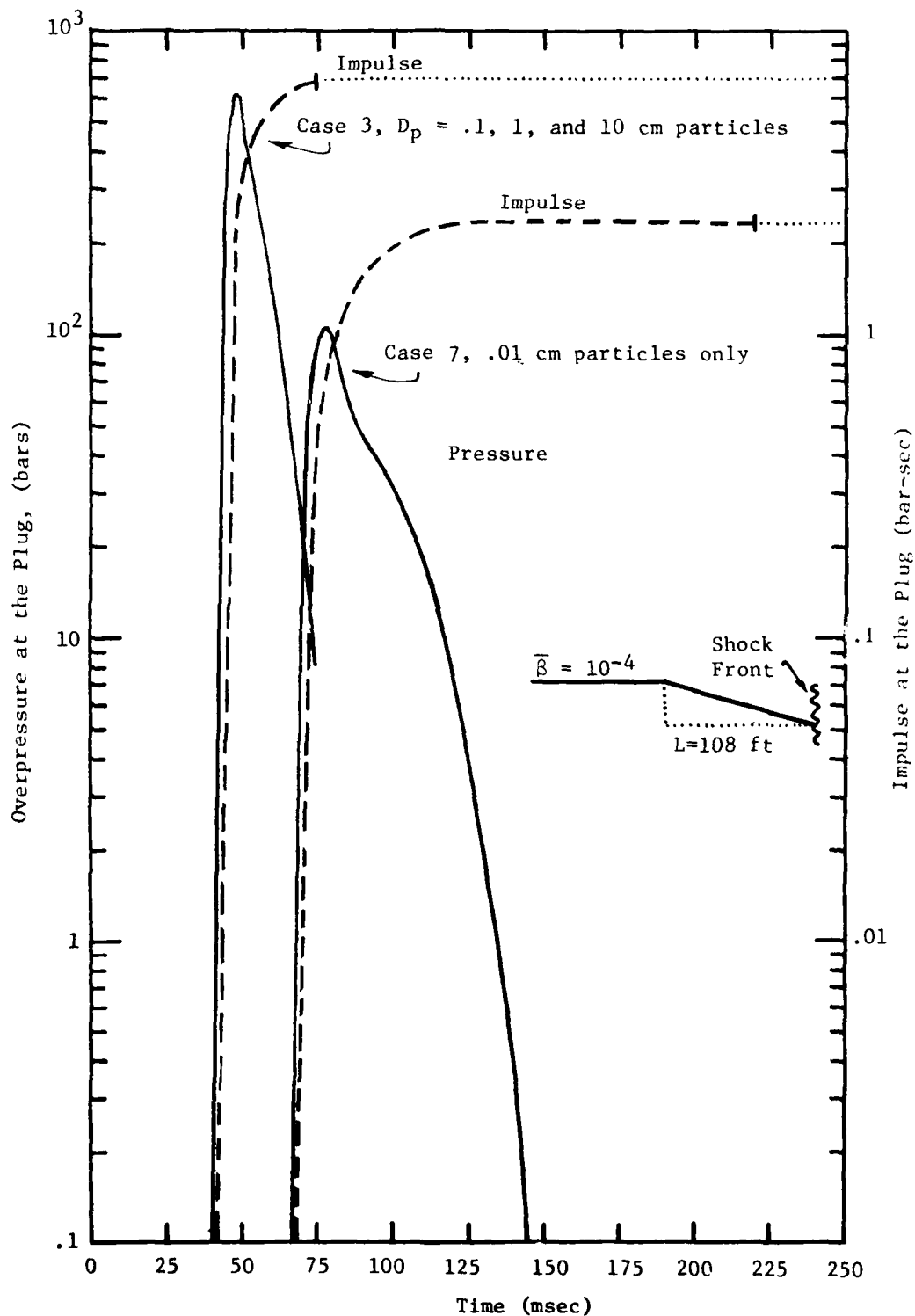


Figure 7. Time Histories of Pressure Delivered to the Plug and Impulse for Variations in the Particle Size Distribution ( $\bar{\beta}=10^{-4}$  and  $L=108$  ft using a ramped loading function).

---

TABLE 2. Maximum Pressures and Impulses Delivered to the Plug for Variations in Particle Size Distribution and Thermal Interaction

Case	Thermal Model Active?	Particle Size Distribution $D_p$ (cm)	Maximum Pressure $P_M$	Maximum Impulse $I_M$
3	Yes	.1, 1, and 10 *	621	6.4
7	Yes	.01	107	2.4
8	No	.1, 1, and 10 *	690	6.9
9	No	.01	136	3.7

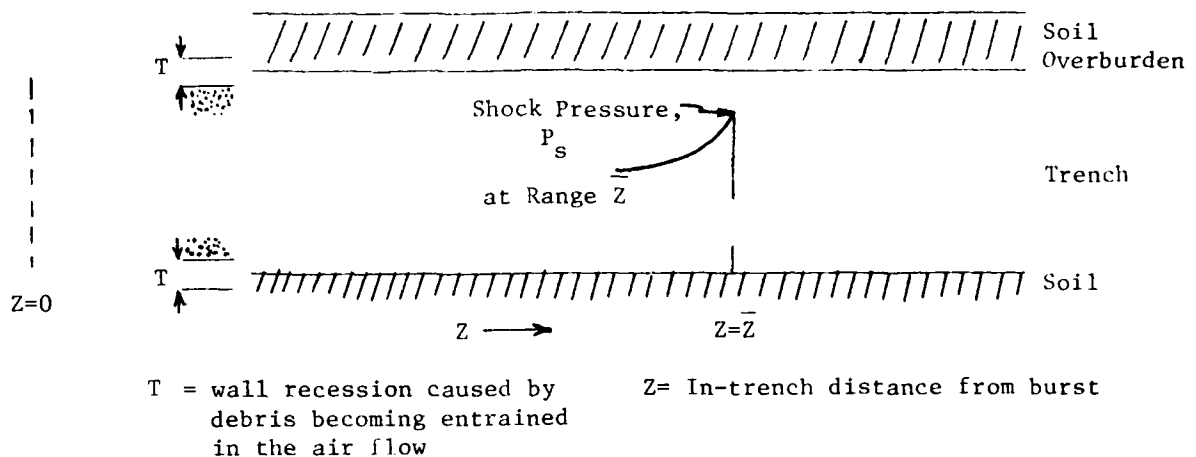
\* Mass is divided equally among .1, 1, and 10 cm particles in these cases.

---

Table 2 indicates that the in-trench mixed phase flow dynamics are dominated by drag interactions as opposed to thermal interactions. The maximum pressure is changed by a factor of only -1.2 when the thermal model is turned off and the initial particle size distribution is held constant (compare Case 3 to Case 8 and Case 7 to Case 9). Thus, the entrained wall debris mass and particle size distributions are important in determining the plug loading characteristics ( $P_M$ ,  $I_M$ ).

## SECTION IV

### IN-TRENCH RESPONSE



#### 4.1 SHOCK PRESSURE ATTENUATION

The shock pressure attenuation curves are obtained from the numerical simulations by plotting the shock pressure and associated range at a series of times, as sketch below:

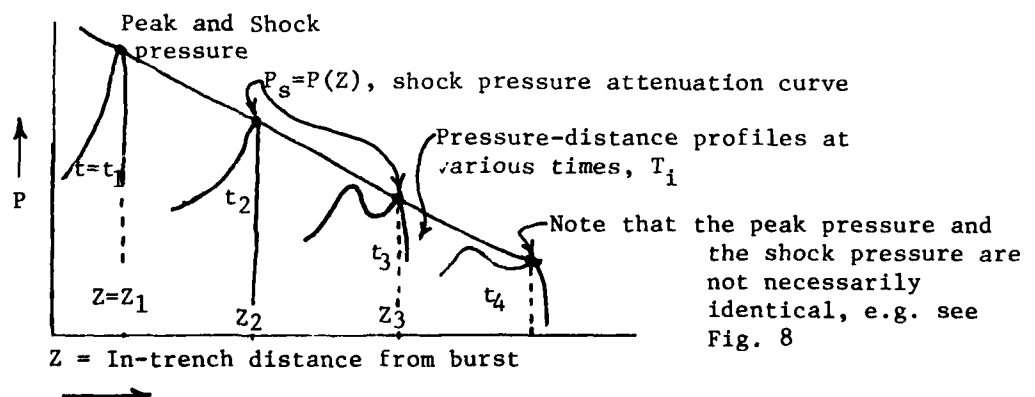


Figure 8 shows the shock pressure attenuation curves and examples of predicted pressure profiles for two debris entrainment lengths of  $L = 18$  feet and 108 feet using a step entrainment function with  $\bar{\beta} = 10^{-3}$  (Case 10 vs Case 2). Note that the attenuation in the two cases is very different. Also, the qualitative nature of the pressure profiles is different. When  $L = 18$  feet, the additional entrained mass near the shock front causes the *peak* pressure to (1) decay much more rapidly as compared to the  $L = 108$  feet case, and (2) occur behind the shock front.

Figure 9 shows the effect of varying the mass loading rate parameter,  $\bar{\beta}$ , for the step entrainment function with  $L = 18$  feet. This figure shows the shock pressure attenuation curves for  $\bar{\beta} = .01$ ,  $.001$ , and  $.0001$ .

Figure 10 indicates the effect of wall debris *particle size* on the shock pressure attenuation characteristics. In most of the cases performed in this study, the wall debris was assumed to enter the air flow with 1 mm, 1 cm, and 10 cm particle diameters. The three sizes were evenly distributed according to mass; however, on Figure 10, two cases are shown where the wall debris was assumed to consist of only 100 micron (.01 cm) particles. As Figure 10 shows, the 100 micron particles are very effective in attenuating the shock pressures; this attenuation is primarily due to particle-air drag interactions. Thus, "fast" mixing of small particles with the shock air will be effective in attenuating the shock pressures in the trench.

#### 4.2 WALL RECESSION

Figure 11 shows two comparisons of wall recession thickness versus distance profiles. In the upper portion of this figure, (Figure 11a) the wall recession versus distance profiles are compared for  $\bar{\beta} = 10^{-3}$  and  $\bar{\beta} = 10^{-4}$  with a step entrainment

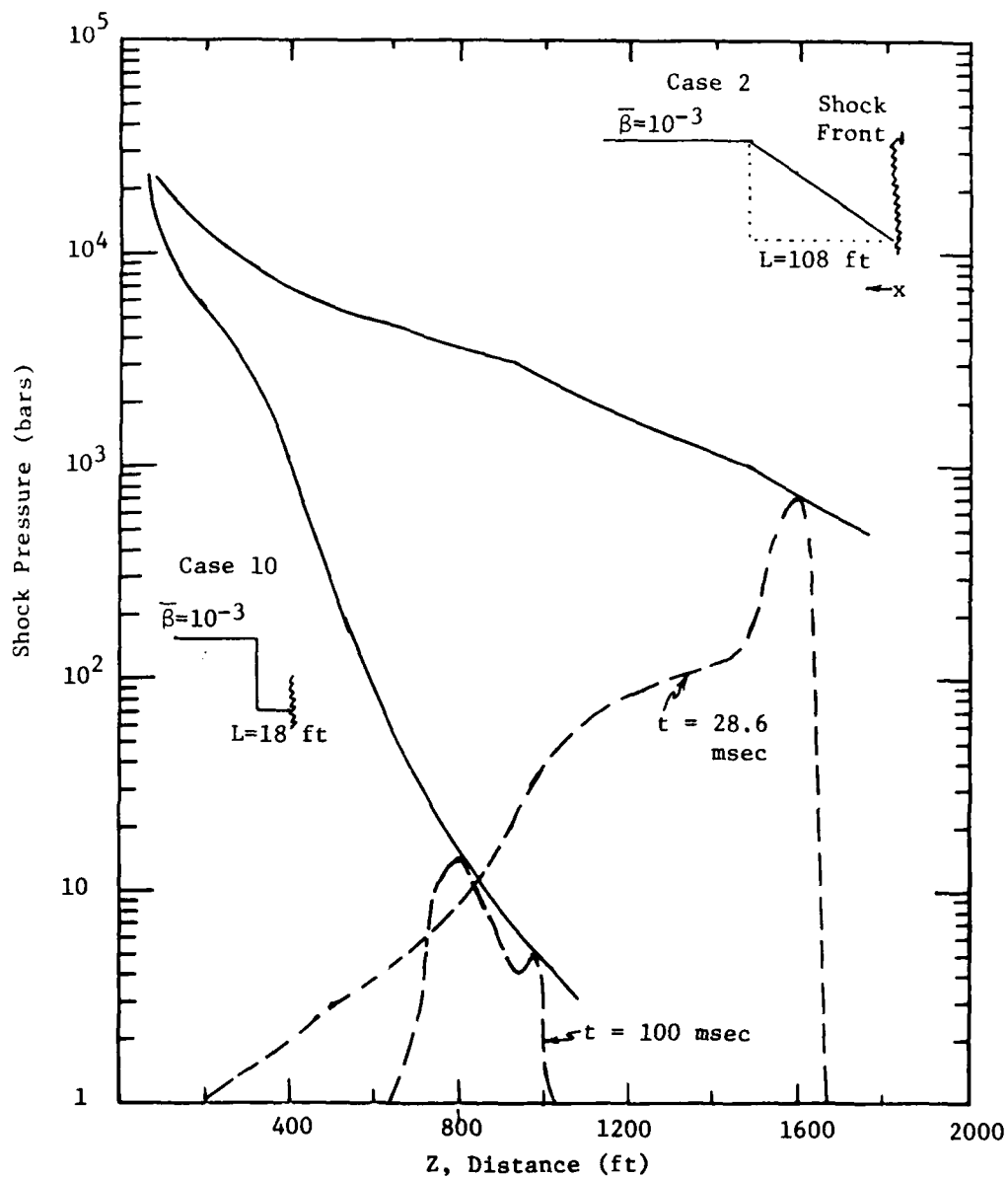


Figure 8. Shock Pressure vs Distance Attenuation Curves for the L=18 ft (Case 10) and L=108 ft (Case 2) Cases Using a Step Entrainment Function with  $\bar{\beta} = 10^{-3}$ . (Dashed curves are Pressure vs Distance Profiles at indicated times.)

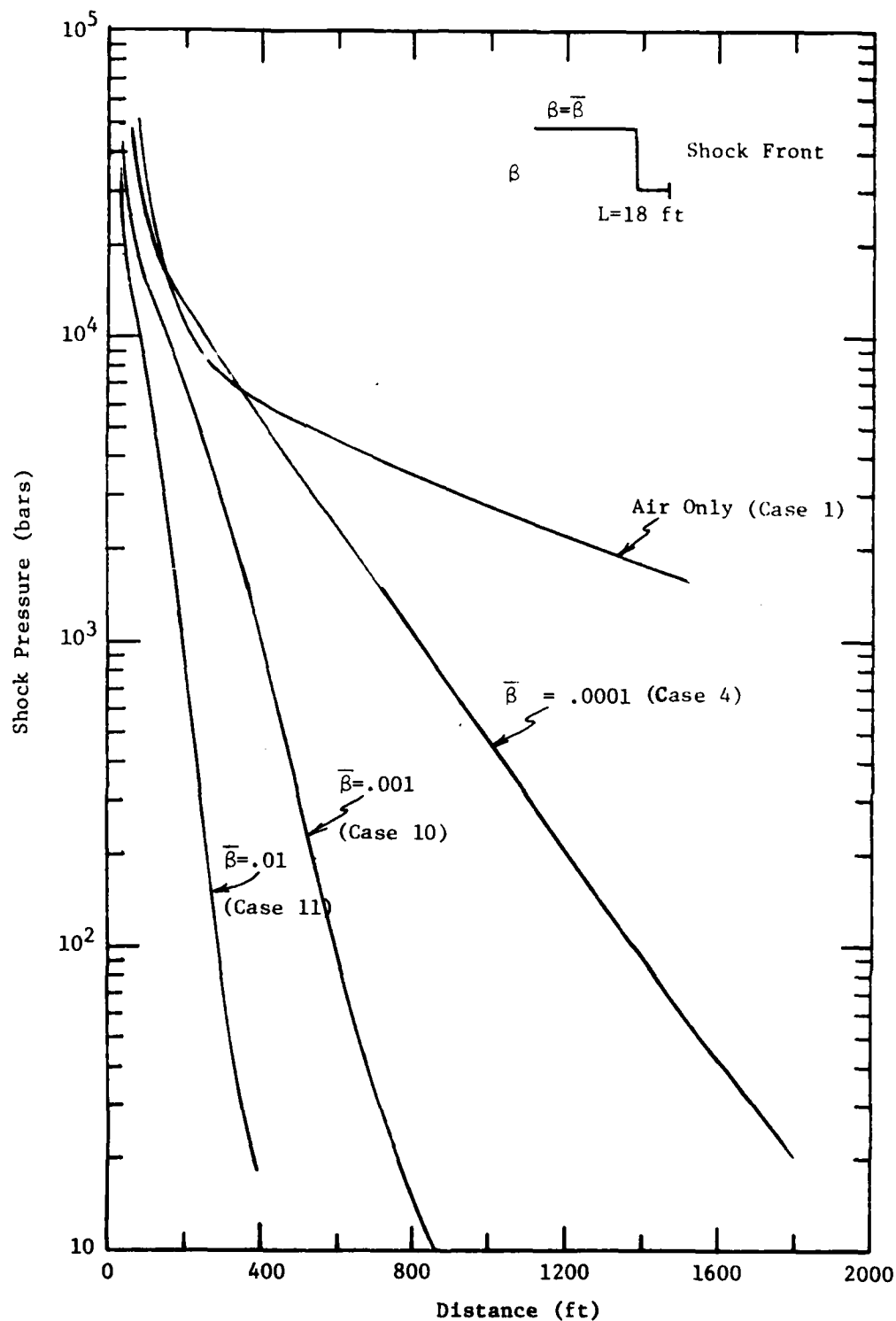


Figure 9. Shock Pressure vs Distance for Various Wall Debris Entrainment Parameters,  $\bar{\beta} = .01$ ,  $.001$ , and  $.0001$  ( $L = 18$  ft,  $\beta$  is a step function).

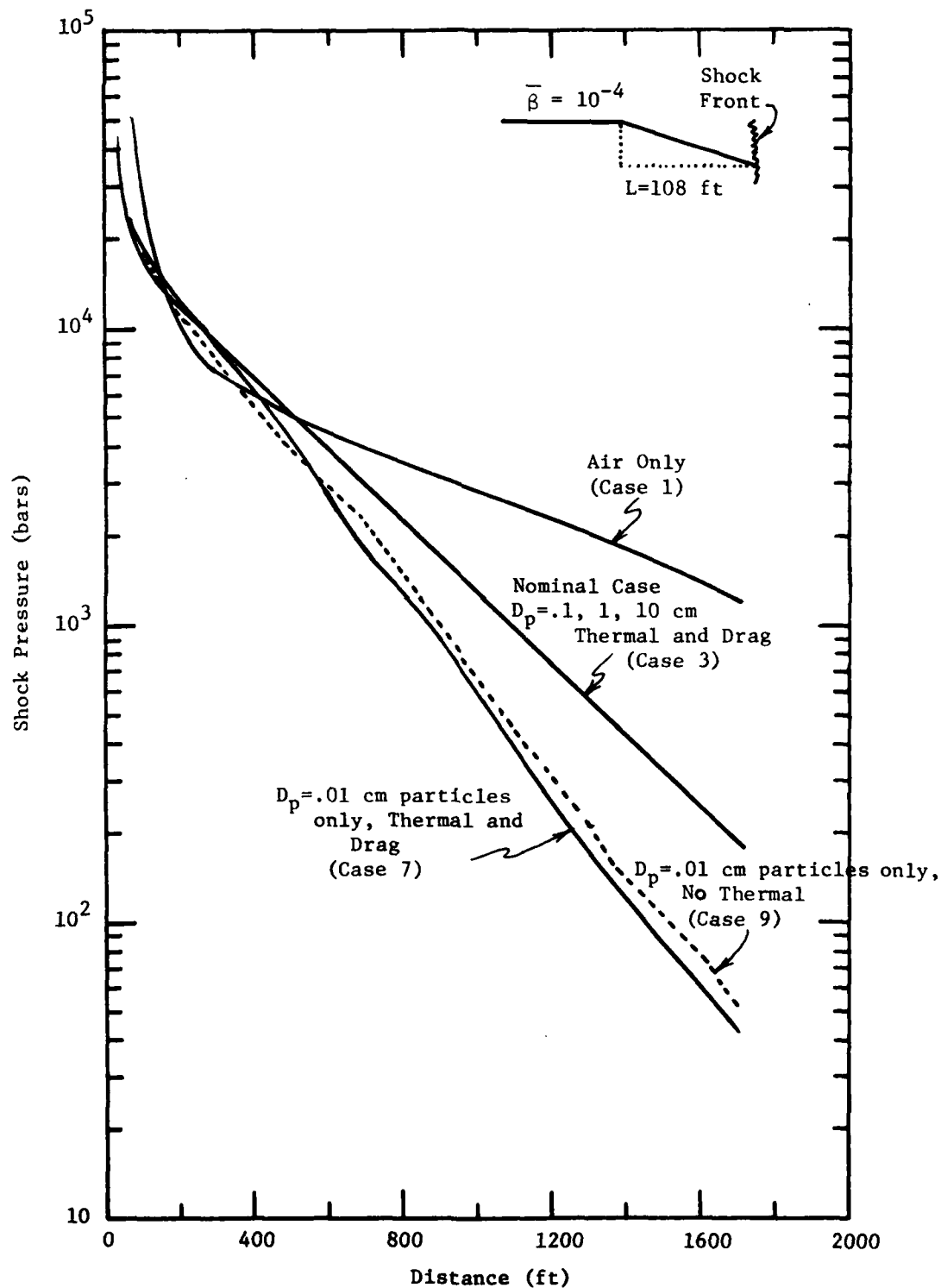


Figure 10. Shock Pressure Attenuation with Distance for Variations in Entrained Particle Size Distribution ( $\bar{\beta} = 10^{-4}$  and  $L = 108 \text{ ft}$  using a Ramped Loading Function).



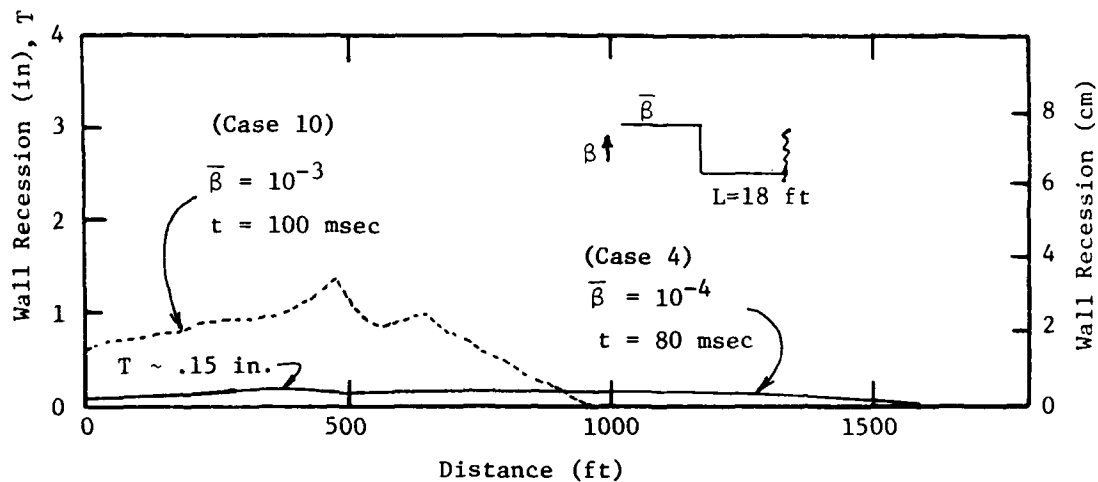


Figure 11a. Wall Recession vs Distance Profiles for  $\bar{\beta} = 10^{-3}$  and  $\bar{\beta} = 10^{-4}$  ( $L=18$  feet with Step Loading Function).

(Note Change in Scale)

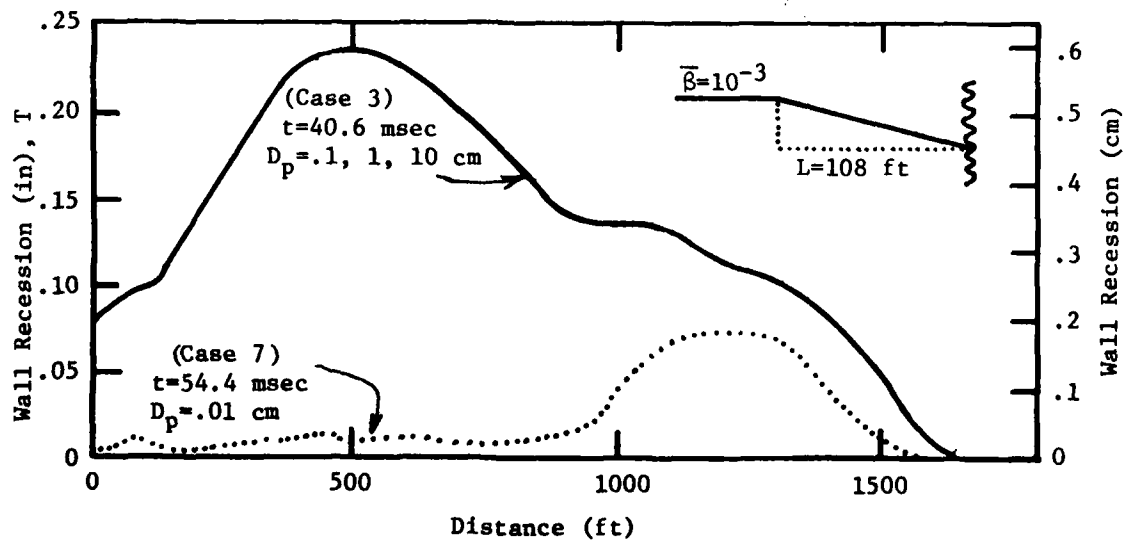


Figure 11b. Wall Recession vs Distance Profiles with Entrained Particle Distributions of  $D_p = .01$  cm and  $D_p = .1, 1, 10$  cm ( $\bar{\beta}=10^{-4}$  and  $L=108$  ft with Linear Loading Function).

function and  $L=18$  feet. Note that even the fraction of an inch recession ( $T \sim .15$  in.) in the  $\bar{\beta} = 10^{-4}$  case (Case 4) causes the maximum pressure at the plug to drop to 80 bars as compared to the  $\sim 6800$  bars in the air-only case (Case 1).

Figure 11b compares the wall recession profiles for a variation in debris particle size (Case 7 vs 3). In Case 7, the wall debris particle diameters are entirely 100 microns = .01 cm. In Case 3, the nominal particle size distribution of  $D_p = .1, 1, \text{ and } 10$  cm is used for the entrained wall debris. Note that in the 100 micron case, less mass has been scoured off the walls, but the attenuation with distance is greater, as previously shown on Figure 10.

## APPENDIX A

### PHYSICAL MODELS USED IN $1\frac{1}{2}$ -D DICE CALCULATIONS

A  $1\frac{1}{2}$ -D calculation can be used to simulate a flow problem that satisfies two conditions:

1. There is a "well-defined" principal flow direction.
2. Transfer of mass, momentum, and energy transverse to the principal flow direction can be modeled so that numerical integrations are only performed in the principal flow direction.

Within the context of the present parametric analyses of mixed phase flow in trenches, these conditions are adequately satisfied during most of the in-trench flow dynamics. These conditions are not satisfied, however, when the trench roof displacement approaches the trench radius in size. Therefore, the  $1\frac{1}{2}$ -D analyses are probably poor simulations near the burst point.

The physical models described in this section are of two types:

1. General Physical Models
  - Drag Model
  - Heat Exchange Model
2. Models for Treating Effects of Transverse Flow Interactions.
  - Venting Model
  - Wall Expansion Model

(The debris entrainment model, which falls in this group, is described in Section II of the text.)

## A.1 AERODYNAMIC DRAG

In DICE mixed phase flow calculations, the dirt particles and air experience mutual drag interactions. The basic model used for the DICE drag interaction force ( $F_D$ ) on a particle of diameter ( $D_p$ ) moving with velocity ( $\vec{V}_p$ ) in a gas stream of density ( $\rho_g$ ) and velocity ( $\vec{V}_g$ ) is:

$$F_D = \frac{1}{2} \rho_g |\vec{V}_p - \vec{V}_g| |\vec{V}_p - \vec{V}_g| C_D \left( \frac{\pi D_p^2}{4} \right) \quad (A.1)$$

where the drag coefficient ( $C_D$ ) is defined by:

$$C_D = 0.6 + \frac{36}{Re} \quad (A.2)$$

and  $Re$  is the particle Reynold's number,

$$Re = \frac{D_p |\vec{V}_p - \vec{V}_g| \rho_g}{\mu} \quad (A.3)$$

where

$$\mu = (2.42T)^{0.78} \times 10^{-6} \text{ poise, } T \text{ in } ^\circ K$$

The relative masses of particles and gas in a computational cell are used to guarantee that changes in the dirt particle momentum are compensated by oppositely-directed changes in the air momentum (see Reference 2 for additional details).

## A.2 THERMAL INTERACTION

The DICE thermal interaction model couples dirt particle ablation, condensation, and internal heat conduction with changes in the air internal energy. Energy is exchanged between the gas phase (air and dirt vapor) and condensed dirt particles by black body radiation and convection. The convective exchange model

includes the effects of the strong radial gas flow that accompanies small particle ablation or condensation. For a complete discussion of the DICE thermal interaction model, refer to Appendix C of Reference 4.

Sample radiative and convective extinction times for dirt particles at a gas temperature of 20,000°K (also assuming  $P=1$  kbar,  $Re=10^4$ , and a small dirt to air mass ratio) are shown in Figure 12. An extinction time is the time required for a dirt particle of a given initial diameter to ablate completely at constant gas temperature. Observe that the convective extinction time varies as the square of the particle diameter while the radiative extinction time varies as the particle diameter. Thus the 100 $\mu$  particles have radiative extinction times of about 300  $\mu$ sec as compared to 3 msec for 1 mm particles.

### A.3 1½-D VENTING AND WALL EXPANSION

Roof venting and trench wall expansion are coupled in the 1½-D DICE solutions. An equivalent square trench is defined as shown in Figure 13, parts a and b. The width (W) of a square trench equivalent in cross-sectional area to a cylindrical trench of radius ( $R_0$ ) is defined by

$$W = \sqrt{\pi} R_0 \quad (A.4)$$

H is the combined roof and overburden thickness of mean density ( $\rho_s$ ).

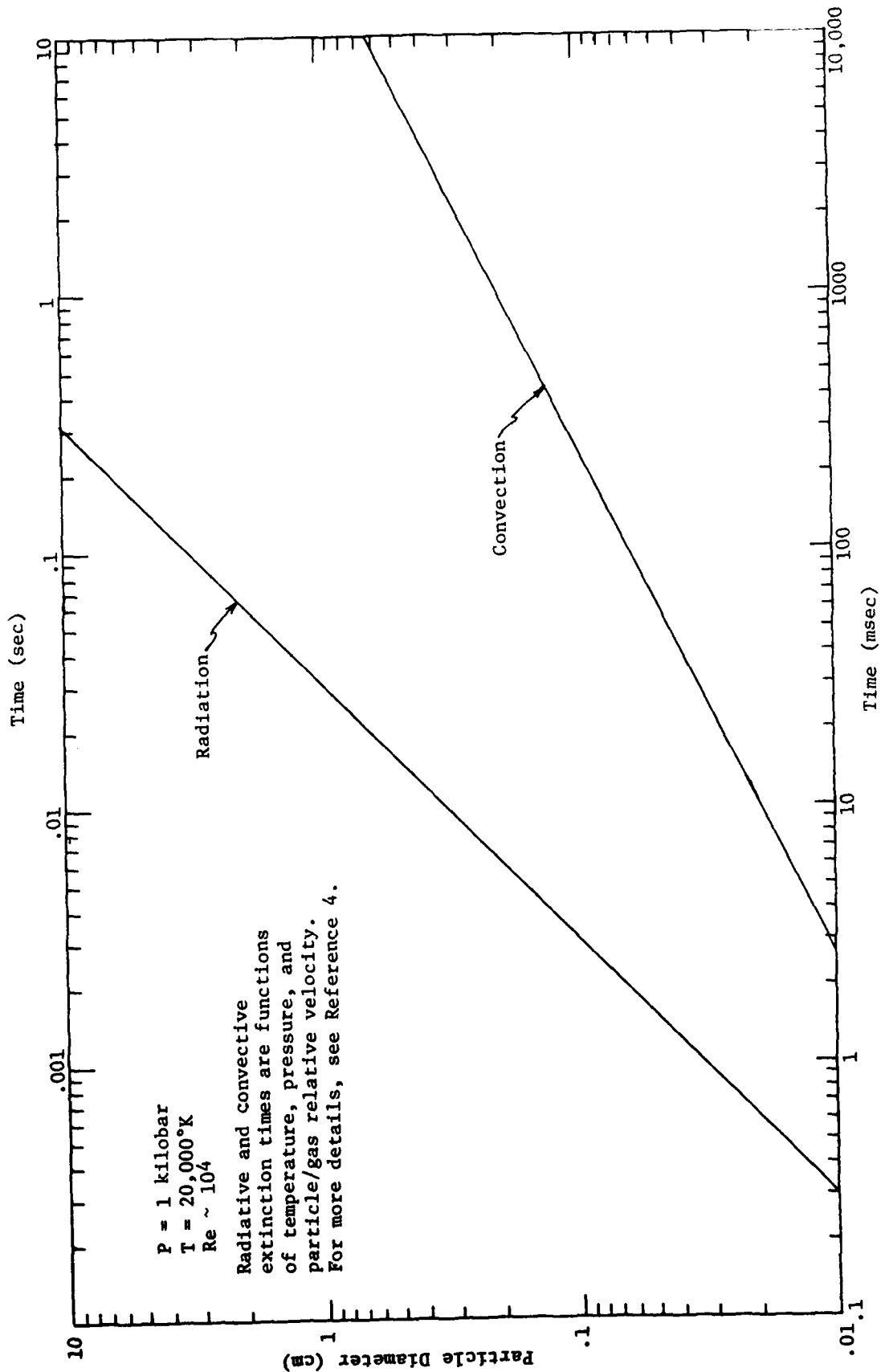


Figure 12. Extinction Times versus Particle Diameter for Radiative and Convective Heat Transfer Assuming a Small Dirt to Air Mass Ratio.

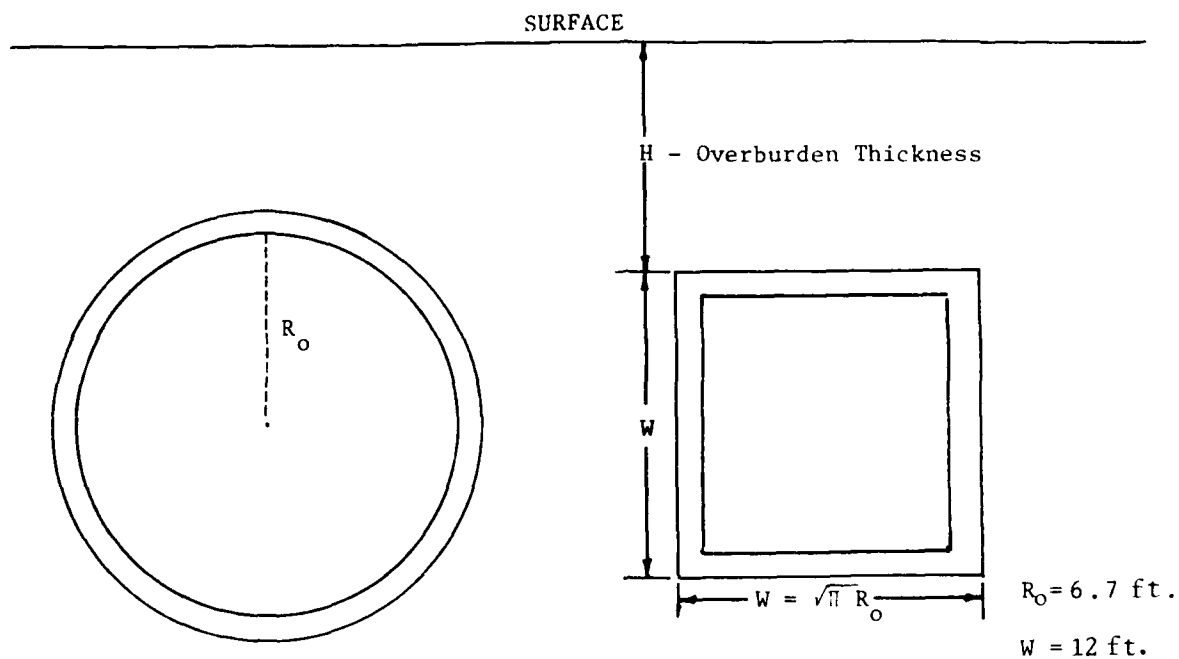


Figure 13a. Equivalence of Circular and Square Trench Crosssections

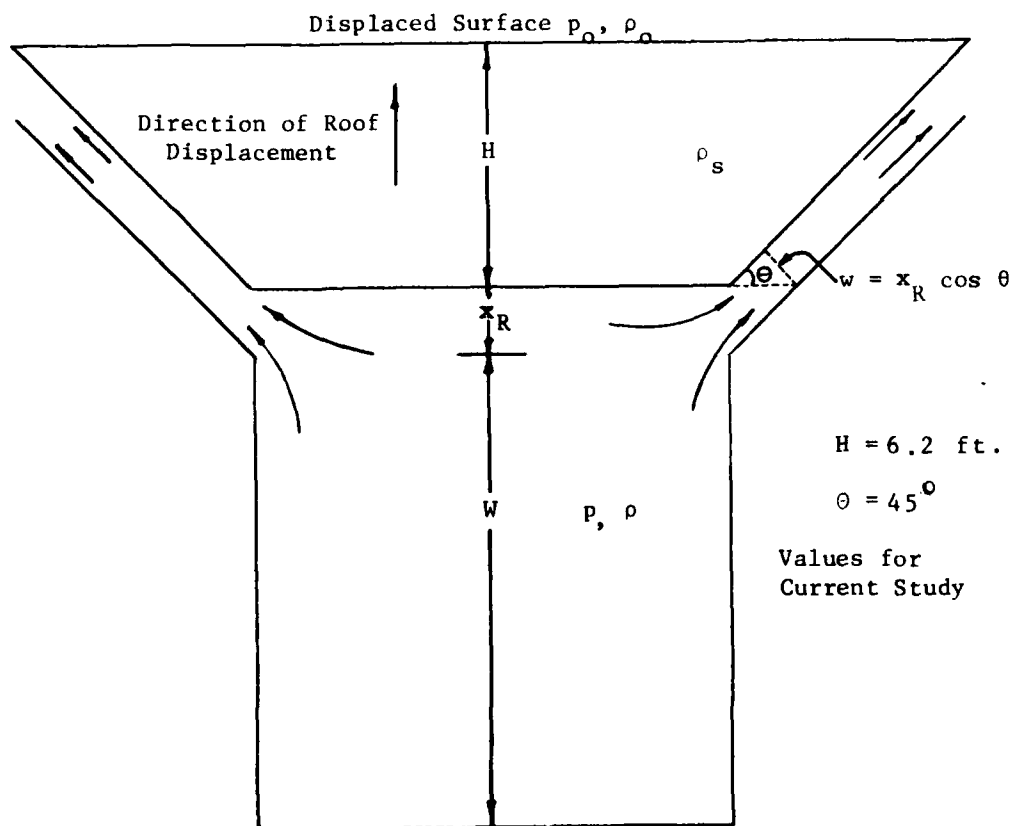


Figure 13b. Wall Expansion and Venting of Equivalent Square Trench

The models assume that the roof displaces upward (with rigid body displacement  $x_R$ ) as a trapezoidal wedge and that the trench gases vent through the resulting channel of width ( $w$ ). The moving roof obeys the simple equation of motion.

$$\ddot{x}_R = \frac{p-p_0}{\rho_s H} \quad (A.5)$$

If  $p$  is constant during an integration cycle, the roof velocity and displacement are:

$$\dot{x}_R = \frac{(p-p_0)}{\rho_s H} t + \dot{x}_{R_0} \quad (A.6)$$

$$x_R = \frac{(p-p_0)}{2\rho_s H} t^2 + \dot{x}_{R_0} t + x_{R_0} \quad (A.7)$$

where  $\dot{x}_{R_0}$  and  $x_{R_0}$  are the roof velocity and displacement at the beginning of the integration cycle.

The trench is modeled as completely open when the vent channel area equals the trench roof area or when

$$x_R = W/2\cos\theta \quad (A.8)$$

Prompt venting is assumed to occur for all non-zero values of  $x_R$ .

The vent fraction ( $\eta$ ) is defined as the ratio of vent area to equivalent square trench roof area,

$$\eta = 2x_R\cos\theta/W \quad (A.9)$$



The venting velocity ( $V_o$ ) is standardly (Reference 5 ) defined by

$$V_o = \eta G \left[ \frac{2(p-p_o)}{\rho} \right]^{1/2} \quad (A.10)$$

where  $G$  is the ventilation coefficient ( $G = .711$ ) and  $\rho$  is the trench gas density.

The mass outflow rate per unit length ( $\dot{m}_o$ ) is

$$\dot{m}_o = \rho V_o w = \frac{4Gx_R^2 \cos^2 \theta}{w} [2(p-p_o)\rho]^{1/2} \quad (A.11)$$

If the venting velocity exceeds the local trench sound speed ( $c$ ), the venting flow is assumed to choke at speed  $c$ . In this case

$$\dot{m}_o = \rho c w = 2\rho c x_R \cos \theta, \quad V_o > c \quad (A.12)$$

The radius ( $R$ ) of an expanding cylindrical tunnel was modeled by letting

$$R^2 = R_o^2 \left( 1 + \frac{x_R}{w} \right) \quad (A.13)$$

The change in total gas density in the trench due to venting and wall expansion can then be expressed by

$$\dot{\rho} = \dot{\rho}_{\text{vent}} + \dot{\rho}_{\text{expansion}} \quad (A.14)$$

where

$$\dot{\rho}_{\text{vent}} = - \frac{\dot{m}_o}{\pi R^2} \quad (A.15)$$

and

$$\dot{\rho}_{\text{expansion}} = - \frac{2\rho \dot{R}}{R} \quad (A.16)$$

## REFERENCES

1. "MX Weapon Systems Concept Validation Phase Survivability Program Plan," Prepared by the Department of the Air Force Space and Missile System Organization (SAMSO) Deputy for Intercontinental Ballistic Missiles, Norton AFB, CA, September 1976.
2. M. Rosenblatt, G. E. Eggum, March 1973, Private Communication.
3. M. Rosenblatt, G. E. Eggum, May 1975, Private Communication.
4. M. Rosenblatt, G. Carpenter and G. Eggum, Sept. 1975, Private Communication.
5. L. M. Milne-Thomson, "Theoretical Hydrodynamics," MacMillan, 1965.

## DISTRIBUTION LIST

### DEPARTMENT OF DEFENSE

Assistant to the Secretary of Defense  
Atomic Energy  
ATTN: Executive Assistant

Defense Advanced Rsch. Proj. Agency  
ATTN: TIO

Defense Intelligence Agency  
ATTN: RDS-3A

Defense Nuclear Agency  
ATTN: DDST  
ATTN: SPSS, G. Ullrich  
ATTN: SPSS, E. Sevin  
3 cy ATTN: SPSS, J. Galloway  
4 cy ATTN: TITL

Defense Technical Information Center  
12 cy ATTN: DD

Field Command  
Defense Nuclear Agency  
ATTN: FCTMD  
ATTN: FCPR

Field Command  
Defense Nuclear Agency  
Livermore Division  
ATTN: FCPRL

Joint Strat. Tgt. Planning Staff  
ATTN: XPFS  
ATTN: NRI-STINFO Library

Undersecretary of Def. for Rsch. & Engrg.  
ATTN: Strategic & Space Systems (OS)

### DEPARTMENT OF THE ARMY

BMD Advanced Technology Center  
Department of the Army  
ATTN: ATC-T

Chief of Engineers  
Department of the Army  
ATTN: DAEN-RDM  
ATTN: DAEN-RDL  
ATTN: DAEN-MPE-T, D. Reynolds  
ATTN: DAEN-ASI-L

Harry Diamond Laboratories  
Department of the Army  
ATTN: DELHD-N-P  
ATTN: DELHD-I-TL

U.S. Army Ballistic Research Labs.  
ATTN: DRDAR-BLE, J. Keefer  
ATTN: DRDAR-TSB-S

U.S. Army Cold Region Res. Engr. Lab  
ATTN: Library

U.S. Army Construction Engrg. Res. Lab.  
ATTN: Library

### DEPARTMENT OF THE ARMY (Continued)

U.S. Army Engineer Center  
ATTN: Technical Library

U.S. Army Engr. Waterways Exper. Station  
ATTN: WESSD, G. Jackson  
ATTN: Library  
ATTN: WESSA, W. Flathau

U.S. Army Material & Mechanics Rsch. Ctr.  
ATTN: Technical Library

U.S. Army Materiel Dev. & Readiness Cmd.  
ATTN: DRXAM-TL

U.S. Army Nuclear & Chemical Agency  
ATTN: Library

### DEPARTMENT OF THE NAVY

Naval Construction Battalion Center  
Civil Engineering Laboratory  
ATTN: Code L51, J. Crawford  
ATTN: Code L08A  
ATTN: Code L53, J. Forrest

Naval Facilities Engineering Command  
ATTN: Code 09M22C

Naval Postgraduate School  
ATTN: Code 0142  
ATTN: G. Lindsay

Naval Research Laboratory  
ATTN: Code 2627

Naval Surface Weapons Center  
ATTN: Code X211  
ATTN: Code F31

Naval Surface Weapons Center  
ATTN: Tech. Library & Info. Services Branch

Office of Naval Research  
ATTN: Code 715

### DEPARTMENT OF THE AIR FORCE

Air Force Institute of Technology  
Air University  
ATTN: Library

Headquarters  
Air Force Systems Command  
ATTN: DLWM

Air Force Weapons Laboratory, AFSC  
ATTN: NT, D. Payton  
ATTN: DE, M. Plamondon  
ATTN: DED-I  
ATTN: DED-A  
ATTN: SUL  
ATTN: DES-S  
ATTN: DES-G  
ATTN: DEO  
ATTN: DEY

DEPARTMENT OF THE AIR FORCE (Continued)

Assistant Chief of Staff  
Intelligence  
Department of the Air Force  
ATTN: IN

Assistant Secretary of the AF  
Research, Development & Logistics  
Department of the Air Force  
ATTN: SAFALR/DEP for Strat. & Space Sys.

Ballistic Missile Office  
Air Force Systems Command  
ATTN: MNXX, W. Crabtree  
ATTN: MNXH, D. Gage

Deputy Chief of Staff  
Research, Development & Acq.  
Department of the Air Force  
ATTN: AFRDQA  
ATTN: AFRDPN  
ATTN: AFRD-M, L. Montulli  
ATTN: AFRDQSM

Strategic Air Command  
Department of the Air Force  
ATTN: XPFS  
ATTN: NRI-STINFO Library

Vela Seismological Center  
ATTN: G. Ullrich

OTHER GOVERNMENT AGENCY

Federal Emergency Management Agency  
ATTN: Hazard Eval. & Vul. Red. Div., G. Sisson

DEPARTMENT OF ENERGY CONTRACTORS

Lawrence Livermore Laboratory  
ATTN: Document Control for D. Glenn

Los Alamos Scientific Laboratory  
ATTN: Document Control for C. Keller  
ATTN: Document Control for R. Sanford

Sandia Laboratories  
ATTN: Document Control for Org. 1250, W. Brown  
ATTN: Document Control for A. Chabai

DEPARTMENT OF DEFENSE CONTRACTORS

Acurex Corp.  
ATTN: C. Wolf  
ATTN: K. Triebes  
ATTN: J. Stockton

Aerospace Corp.  
ATTN: Technical Information Services  
ATTN: H. Mirels

Agabian Associates  
ATTN: M. Agabian

Applied Theory, Inc.  
2 cy ATTN: J. Trulio

Boeing Co.  
ATTN: Aerospace Library  
ATTN: S. Strack

DEPARTMENT OF DEFENSE CONTRACTORS (Continued)

California Research & Technology, Inc.  
ATTN: Library  
ATTN: M. Rosentblatt  
ATTN: G. Carpenter  
ATTN: R. Bilyeu

Civil Systems, Inc.  
ATTN: J. Bratton

Civil Systems, Inc.  
ATTN: S. Melzer

Erich H. Wang  
Civil Engineering Rsch. Fac.  
ATTN: J. Kovarna  
ATTN: P. Lodde

General Electric Company-TEMPO  
ATTN: DASAC

H-Tech Labs, Inc.  
ATTN: B. Hartenbaum

Higgins, Auld & Associates  
ATTN: N. Higgins  
ATTN: H. Auld

IIT Research Institute  
ATTN: Documents Library

J. H. Wiggins Co., Inc.  
ATTN: J. Collins

Merritt CASES, Inc.  
ATTN: Library

Nathan M. Newmark Consult. Eng. Svcs.  
ATTN: N. Newmark  
ATTN: W. Hall

Pacific-Sierra Research Corp.  
ATTN: H. Brode

Mission Research Corp.  
ATTN: C. Longmire  
ATTN: G. McCartor

Pacifica Technology  
ATTN: Library  
ATTN: R. Allen

Physics International Co.  
ATTN: Technical Library  
ATTN: J. Thomsen  
ATTN: F. Sauer

R & D Associates  
ATTN: J. Lewis  
ATTN: Technical Information Center  
ATTN: C. MacDonald  
ATTN: R. Port  
ATTN: J. Carpenter

Science Applications, Inc.  
ATTN: H. Wilson  
ATTN: R. Schlaug  
ATTN: Technical Library

Science Applications, Inc.  
ATTN: D. Hove

DEPARTMENT OF DEFENSE CONTRACTORS (Continued)

Science Applications, Inc.  
ATTN: B. Chambers III

SRI International  
ATTN: G. Abrahamson  
ATTN: Library  
ATTN: J. Colton

Systems, Science & Software, Inc.  
ATTN: Library  
ATTN: C. Dismukes  
ATTN: K. Pyatt  
ATTN: J. Barthel

Systems, Science & Software, Inc.  
ATTN: J. Murphy

Systems, Science & Software, Inc.  
ATTN: C. Hastings

DEPARTMENT OF DEFENSE CONTRACTORS (Continued)

Systems, Science & Software, Inc.  
ATTN: C. Needham

Terra Tek, Inc.  
ATTN: Library  
ATTN: A. Abou-Sayed

TRW Defense & Space Sys. Group  
ATTN: Technical Information Center  
ATTN: N. Lipner

TRW Defense & Space Sys. Group  
ATTN: G. Hulcher

Weidlinger Assoc., Consulting Engineers  
ATTN: I. Sandler

Weidlinger Assoc., Consulting Engineers  
ATTN: J. Isenberg